Chapter 2
Recent Structural Insights into the Molecular Architecture of Synapses



Axel T. Brunger, Richard G. Held, Yousuf A. Khan, Jeremy Leitz, Jiahao Liang, Chuchu Wang, and K. Ian White

Abstract Synaptic transmission between pre- and postsynaptic neurons occurs when the presynaptic neuron terminal is temporarily depolarized upon action potential arrival, opening voltage-gated Ca^{2+} channels at synapses. Ca^{2+} will flow into the presynapse, and it will trigger the fusion of neurotransmitter-filled synaptic vesicles with the presynaptic membrane in less than a millisecond. Neurotransmitter molecules are then released into the synaptic cleft and bind to receptors in the postsynaptic membrane. Understanding the mechanisms that underlie this complex cellular process requires detailed knowledge of the spatial and structural organization of the macromolecular components of the synapse. This chapter focuses on recent structural insights into the presynaptic machinery and the spatial relationship between synaptic vesicles, presynaptic factors, and postsynaptic receptors.

Keywords Synaptic transmission · Synaptic vesicle fusion · SNARE · Synaptotagmin · Complexin · N-ethylmaleimide-sensitive factor · SNAP · Munc13 · Munc18 · AMPA receptor

---

The original version of the chapter has been revised. A correction to this chapter can be found at https://doi.org/10.1007/978-3-032-12594-1_12

A. T. Brunger (✉) · R. G. Held · Y. A. Khan · J. Leitz · J. Liang · C. Wang · K. I. White
Department of Molecular and Cellular Physiology, Stanford University, Stanford, CA, USA

Department of Neurology and Neurological Sciences, Stanford University, Stanford, CA, USA

Department of Structural Biology, Stanford University, Stanford, CA, USA

Department of Photon Science, Stanford University, Stanford, CA, USA

Howard Hughes Medical Institute, Stanford University, Stanford, CA, USA
e-mail: brunger@stanford.edu

© The Author(s) 2026, Corrected Publication 2026

E. T. Kavalali (ed.), *Nano-organization of the Synapse*, Advances in Neurobiology 48,
https://doi.org/10.1007/978-3-032-12594-1_2

2.1 Introduction

Neuronal synapses are specialized signaling compartments that control information transfer in the nervous system. Synaptic transmission between pre- and postsynaptic neurons occurs when the presynaptic neuron terminal is temporarily depolarized upon action potential arrival, opening voltage-gated Ca^{2+} channels at synapses. Because the extracellular Ca^{2+} concentration is much higher than the basal cytoplasmic concentration, Ca^{2+} will flow into the neuron. In turn, Ca^{2+} will trigger the fusion of neurotransmitter-filled synaptic vesicles with the presynaptic membrane in less than a millisecond (Rothman 2014; Südhof 2013). Neurotransmitter molecules are then released into the synaptic cleft and bind to receptors in the postsynaptic membrane. Essential components of the synaptic vesicle fusion machinery include the neuronal SNAREs (*S*oluble *N*-ethylmaleimide-sensitive factor *A*ttachment protein *RE*ceptor), the Ca^{2+} sensor synaptotagmin, the activator/regulator complexin, the assembly factors Munc18 (*m*ammalian *unc*oordinated-18) and Munc13 (*m*ammalian *unc*oordinated-13), the AAA+ ATPase N-ethylmaleimide-sensitive factor (NSF, Sec18 in lower eukaryotes), and soluble NSF attachment proteins (SNAPs, Sec17 in lower eukaryotes) (Fig. 2.1) and are summarized in references Brunger et al. (2018) and Rizo (2022). In addition, other active zone proteins (including RIM and RIM-BP) connect the voltage-gated Ca^{2+} channel to the fusion machinery and Rab effector proteins, as summarized in references Held

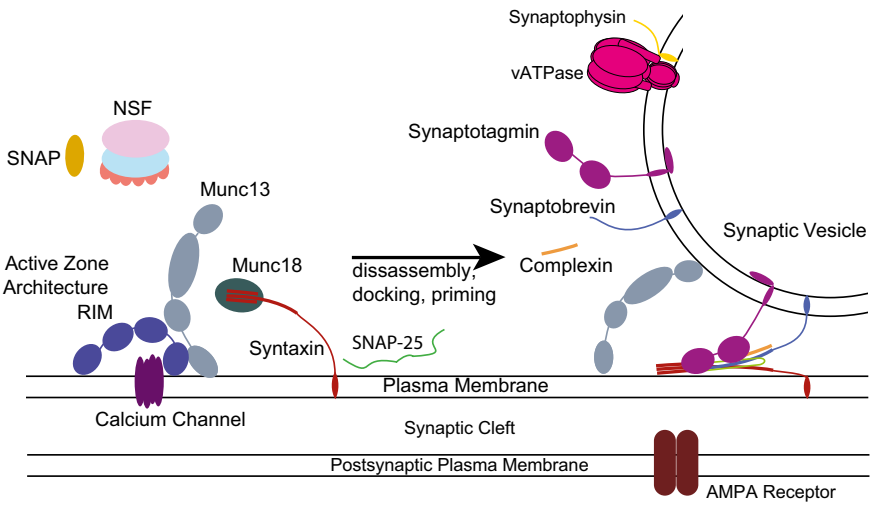


Fig. 2.1 A simplified schema of the presynaptic neurotransmitter release machinery that is discussed in this chapter. Shown are a subset of presynaptic proteins (RIMs, Munc13, Munc18, P/Q- or N-type Ca^{2+}-channels), SNAREs (SNAP-25, syntaxin, and synaptobrevin), complexin, synaptotagmin, NSF, and α-SNAP. Also shown are the synaptic vesicle V-ATPase and synaptophysin, as well as the AMPA receptor in the postsynaptic membrane

and Kaeser (2018) and Südhof (2012). For the proteins in the synaptic cleft and the postsynaptic side, we refer to references Südhof (2012, 2017).

Understanding the mechanisms that underlie this complex cellular process requires detailed knowledge of the spatial and structural organization of the macromolecular components of the synapse. This chapter focuses on recent structural insights into the presynaptic machinery and recent new insights on how these presynaptic factors relate to postsynaptic receptors.

2.2 Technical Developments: Cryo-Electron Tomography and FIB Milling

Recent advances in cryo-electron microscopy (cryo-EM) and tomography (cryo-ET) have been instrumental in the three-dimensional imaging of cellular samples frozen in a near-native state (Turk and Baumeister 2020). These developments have enabled high-resolution in situ structure determination of large protein complexes in cells, including ribosomes, proteasomes, nuclear pore complexes, and muscle sarcomeres (Mosalaganti et al. 2022; Schuller et al. 2021; Tegunov et al. 2021; Wang et al. 2022a). These in situ structures required accurate localization of target proteins within tomographic volumes, relying on their large size, distinctive shape, or ultrastructural arrangement. When successful, subtomogram averaging and in situ structure determination can reveal protein structure and conformation in a native environment, including interactions with known and unknown binding partners. Cryo-ET requires thin enough samples (~100–200 nm thickness) to achieve good image contrast and minimal background. Focused-ion beam (FIB) milling of cryo-frozen samples is often essential to achieve such thin samples. A key advantage of using cryo-fixation is that artifacts due to chemical fixation or freeze substitution techniques can be avoided (Korogod et al. 2015).

In principle, these advances in cryo-ET promise to visualize proteins and uncover the molecular architecture of cells, particularly synapses. However, there are significant challenges to achieving molecular or atomic resolution due to the relatively small size of many synaptic proteins, and their association with membranes can obscure the protein densities. This chapter provides examples illustrating the current state-of-the-art imaging of synapses and synaptic proteins.

2.3 Presynaptic Architecture

Figure 2.2a shows one slice (thickness of ~14 nm) of a 3D cryo-ET reconstruction of a FIB-milled lamella of primary cultures of mouse hippocampal neurons (Held et al. 2024a). On the presynaptic side, many synaptic vesicles are typically observed (Fig. 2.2a) with a bimodal distance distribution to the active zone membrane (Held

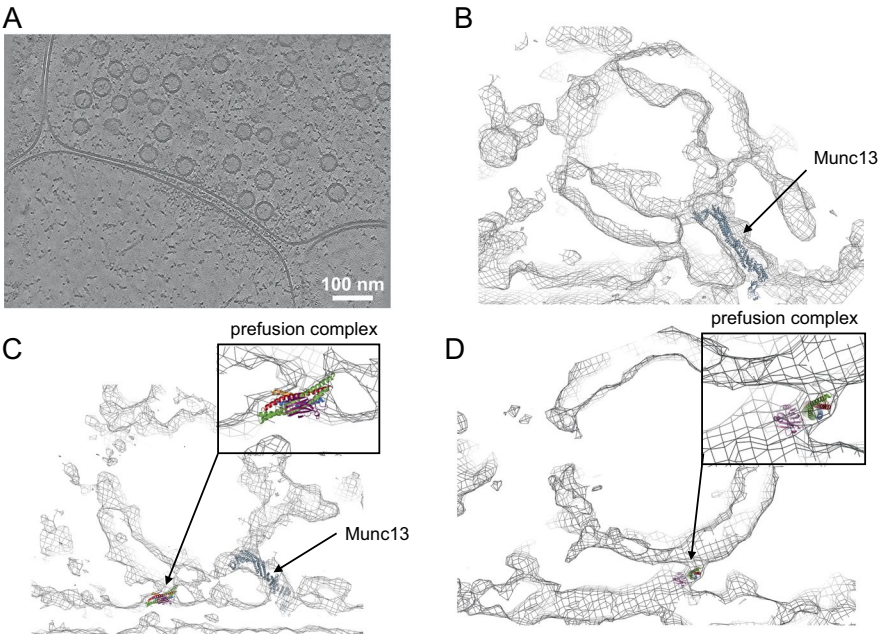


Fig. 2.2 Cryo-ET images of FIB-milled intact synapses (Held et al. 2024a). (**a**) A single XY section through a tomogram of a FIB-milled synapse reconstructed at bin 8 (1.36 nm/pixel) and denoised with cryo-CARE (Buchholz et al. 2018) (TS001 in EMDB EMD-45161) (Held et al. 2024a). (**b**–**d**) Examples of membrane-proximal synaptic vesicles with tether and globular densities. The Wiener-filtered (Tegunov and Cramer 2019) cryo-ET map is shown as a gray mesh at a contour level of 0.5, 0.7, and 1 σ in panels (**b**), (**c**), and (**d**), respectively. The "prefusion complex" (PDB ID 5W5C) (Zhou et al. 2015, 2017), consisting of the SNARE complex (syntaxin: dark red, SNAP-25: green, synaptobrevin: light blue), the C2B domain of synaptotagmin-1 (magenta) interacting with the SNARE complex via the primary interface, and the core domain of complexin-1 (orange), was fitted to globular densities in panels (**c**) and (**d**). The C_1-C_2B-MUN-C_2C fragment of Munc13 (Grushin et al. 2022) (PDB 7T7V, slate blue) was fitted to tether densities in panels (**b**) and (**d**). Munc13 is in an upright position in (**b**) and a lateral position in (**c**). The insets in panels (**c**) and (**d**) show close-up views of the globular densities with the fitted prefusion complex

et al. 2024a). There is a population within less than 10 nm and a broad population beginning at ~10 nm, consistent with previous work; for example, see Imig et al. (2014), which studied the role of priming factors in establishing this distance distribution. The membrane-proximal (<10 nm) synaptic vesicles likely correspond to loosely or tightly primed synaptic vesicles (Lin et al. 2022). In contrast, the more distant synaptic vesicles likely constitute the reserve pool (Denker et al. 2011). However, static cryo-ET reconstructions do not allow one to distinguish between functionally distinct primed/docked synaptic vesicles.

2.4 Intermembrane Densities Between Synaptic Vesicles and the Plasma Membrane

Cryo-ET reconstructions of FIB-milled mouse synapses revealed interfacial densities that connect membrane-proximal synaptic vesicles to the plasma membrane, which can be approximately divided into two broad groups: globular densities and elongated (~20–30 nm long) tethers (Held et al. 2024a) (Fig. 2.2b–d). One to three distinct globular densities were typically observed with no regular or symmetric arrangement. These connecting densities are similar to cryo-ET densities observed in synaptosomes from mouse hippocampal organotypic slice cultures (Orozco-Borunda et al. 2025; Papantoniou et al. 2023) (Fig. 2.3), where, again, no regular arrangements were found. Symmetric arrangements of connecting densities have been reported in subtomogram average maps of cryo-ET reconstructions of cultured hippocampal neurons (Radhakrishnan et al. 2021). However, density maps of individual membrane-proximal synaptic vesicles did not show well-defined regular

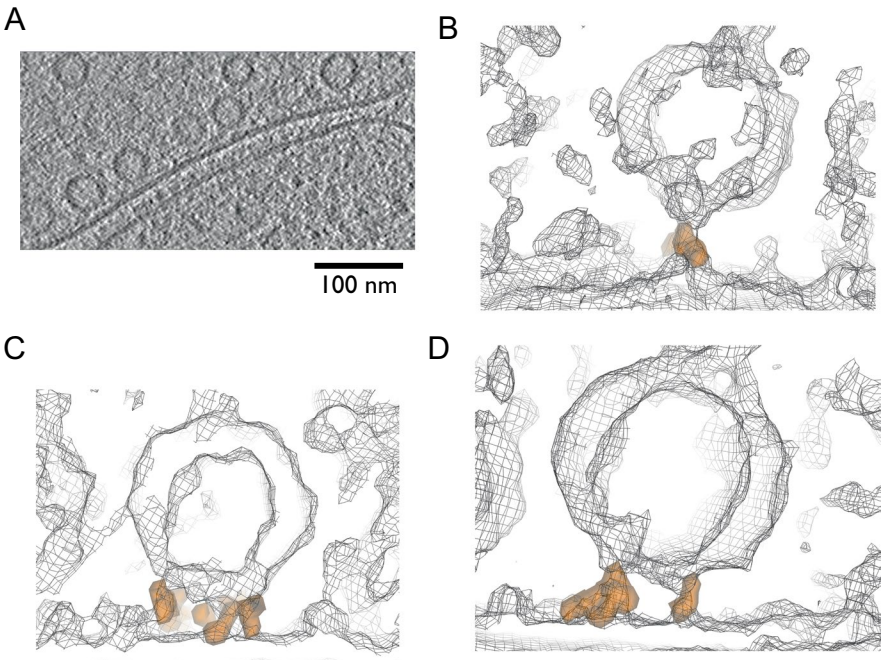


Fig. 2.3 Cryo-ET images of synaptosomes from mouse hippocampal organotypic slice cultures (EMDB EMPIAR-12512) (Orozco-Borunda et al. 2025; Papantoniou et al. 2023). (**a**) A single XY section through a tomogram of a synaptosome at bin 4 (1.756 nm/pixel). (**b**–**d**) Examples of membrane-proximal synaptic vesicles with various densities (orange, detected by Pyto (Lučić et al. 2016)) that connect them to the plasma membrane. The Weiner-filtered (Tegunov and Cramer 2019) cryo-ET map (gray mesh) is shown as a mesh at a contour level of 1, 0.5, and 0.8 σ in panels (**b**), (**c**), and (**d**), respectively

arrangements, which is consistent with the other studies (Held et al. 2024a; Papantoniou et al. 2023).

All these cryo-ET studies support the notion of stable intermembrane densities at resting Ca^{2+} concentrations between synaptic vesicles and plasma membranes. It is tempting to speculate that these complexes occur for primed synaptic vesicles that undergo fast synchronous release, but further experiments are required to investigate this fascinating question. As such, these prefusion complexes are expected to *prevent* fusion since they keep the membranes too far apart for fusion (i.e., more than the critical distance of 0.9 nm) (Aeffner et al. 2012), but they set the stage for fast-triggered fusion upon Ca^{2+} binding to synaptotagmin molecules. As suggested by the recent analyses of neurotransmission of the calyx of Held synapses (Lin et al. 2022), most of these prefusion complexes probably correspond to tightly docked synaptic vesicles.

What are these intermembrane densities? An earlier work revealed similar globular and tether densities using individual cryo-ET reconstructions of synthetic vesicles with reconstituted neuronal SNAREs, synaptotagmin-1, complexin-1, and the C1C2BMUN fragment of Munc13 in the Ca^{2+}-free state (Gipson et al. 2017). The addition of Ca^{2+} resulted in the disappearance of most of these intermembrane densities by vesicle fusion. However, only globular densities were present when Munc13 was omitted. Subsequently, a large cryo-ET dataset of a mixture of isolated glutamatergic synaptic vesicles (ISVs) from a mouse brain homogenate and synthetic vesicles mimicking the plasma membrane was collected in the presence of complexin, but MUN instead of the longer C1C2BMUN fragment (Peters et al. 2022). Subtomogram averages revealed globular, but not tether, densities linking the two types of vesicles (Peters et al. 2022). Again, relatively small numbers of intermembrane densities were observed for a given pair, and there were no apparent regular arrangements between ISVs and acceptor vesicles (Peters et al. 2022). Thus, based on these studies, the globular densities likely contain a "prefusion" complex between neuronal SNAREs, synaptotagmin-1, and complexin-1, especially considering that these were the only proteins used in some conditions in reference Gipson et al. (2017). Recent subtomogram averages of cryo-ET densities observed in synaptosomes from mouse hippocampal organotypic slice cultures (Orozco-Borunda et al. 2025) further support this notion.

What is the molecular composition of the prefusion complex? Before synaptic vesicle fusion, the neuronal SNAREs synaptobrevin-2 (also called VAMP2—*V*esicle *A*ssociated *M*embrane *P*rotein 2) on the synaptic vesicle and syntaxin-1A and SNAP-25A on the plasma membrane initially form a *trans*-SNARE complex (Fig. 2.1), with the transmembrane domains of synaptobrevin-2 and syntaxin-1A in the synaptic vesicle and plasma membranes, respectively. Other synaptic proteins interact with the fully assembled (post-fusion) *cis*-SNARE complex (Chen et al. 2002; White et al. 2018; Zhao et al. 2015; Zhou et al. 2015), and, likely, some of these interactions are also present in the *trans*-SNARE complex (Fig. 2.1).

The crystal structure of the SNARE–synaptotagmin-1–complexin-1 complex (Zhou et al. 2015, 2017) (Fig. 2.4) can fit some of the globular densities (Fig. 2.2c, d) observed in the cryo-ET reconstructions of synapses (Held et al. 2024a). The

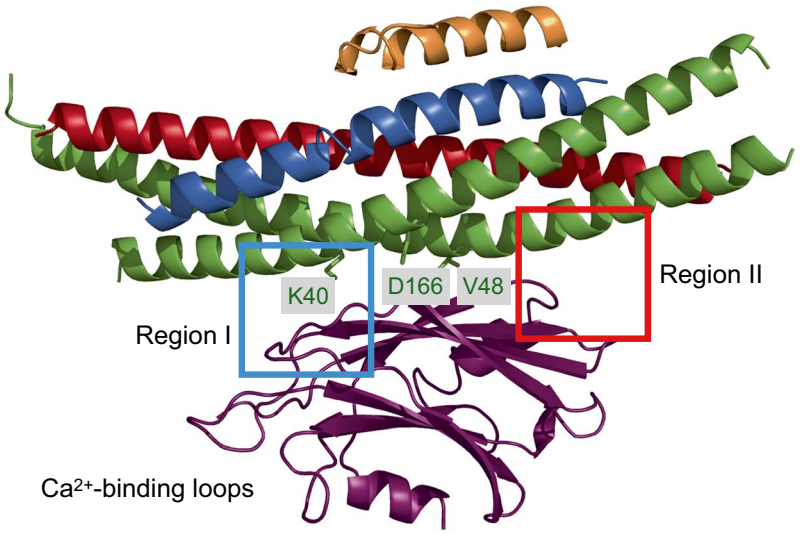


Fig. 2.4 Crystal structure of the SNARE complex (light blue, synaptobrevin-2; dark red, syntaxin-1a; green, SNAP-25) and its interaction with the C2B domain of synaptotagmin-1 (magenta) via the so-called primary interface and its interaction with complexin-1 (orange) (PDB ID 5W5C) (Zhou et al. 2015, 2017). SNAP-25 residues 40, 166, and 48 (sticks) are implicated in DEEs (Alten et al. 2021). Regions I and II of the primary interface (Zhou et al. 2015) are indicated by blue and red rectangles, respectively

structure shown in Fig. 2.4 includes the so-called primary interface between the C2B domain of synaptotagmin-1 and the SNARE complex (Zhou et al. 2015, 2017) and the subcomplex between the SNARE complex and complexin-1 (Chen et al. 2002). Qualitatively similar fits were also obtained using subtomogram average maps obtained from the tomograms of synaptosomes (Orozco-Borunda et al. 2025). The fitted model of the SNARE complex is, of course, an approximation of the expected *trans*-SNARE complex conformation between the synaptic vesicle and plasma membrane. Unfortunately, the tomographic reconstructions and subtomogram averages are not yet of sufficient resolution to determine the details of the *trans*-SNARE complex and its interactions with synaptotagmin and complexin. Nevertheless, these observations are consistent with the notion that the SNARE–synaptotagmin-1–complexin-1 complex is situated between the membrane proximal synaptic vesicles and the plasma membrane in the resting state of the synapse.

As mentioned above, in addition to the globular densities, elongated tether densities were observed in tomographic reconstructions of synapses (Fig. 2.2b, c) (Held et al. 2024a) and in subtomogram average maps of synaptosomes (Orozco-Borunda et al. 2025; Papantoniou et al. 2023). These densities can fit the structures of the C1C2BMUNC2C fragment of Munc13 (Grushin et al. 2022) (Fig. 2.2b, c).

The following sections discuss the prefusion complex and Munc13 in more detail.

2.5 Physiological Relevance of the SNARE—Synaptotagmin-1—Complexin-1 Complex

The primary interface between the SNARE complex and synaptotagmin-1 has an interface area of ~720 Å^2 with a complementary pattern of electrostatic interactions. The primary interface has been observed in several crystallization conditions (Zhou et al. 2015, 2017), in solution by a ^{1}H-^{15}N TROSY-HSQC experiment (Voleti et al. 2020), and by single-particle cryo-EM on lipid nanotubes (Grushin et al. 2019). The primary interface is not close to the Ca^{2+} binding loops of synaptotagmin-1; remarkably, crystal structures in both the absence and presence of Ca^{2+} or Mg^{2+} are very similar (Zhou et al. 2015, 2017). The possible models of Ca^{2+} triggering are discussed below.

The primary interface was tested with a reconstituted fusion assay that included neuronal SNAREs, synaptotagmin-1, and complexin-1 (Zhou et al. 2015). Mutations of both synaptotagmin-1 C2B and SNAP-25A were designed to disrupt the primary interface based on the crystal structures. All mutations disrupted Ca^{2+}-triggered fusion and had varying impacts on vesicle association. Additional support for the primary interface came from electrophysiological experiments of mutations in the C2B domain of synaptotagmin-1 (Zhou et al. 2015, 2017). These mutations disrupted evoked release, while mutations in region II (Fig. 2.4) and the polybasic region increased spontaneous release. All mutations resulted in facilitation during high-frequency stimulation compared to depression for the wildtype cultures. More support came from disease-related mutations of SNAP-25A that are at the primary interface (SNAP-25A Lys40Glu, Asp166Tyr, Val48Phe, Fig. 2.4) (Alten et al. 2021). These particular mutants were uncovered by next-generation DNA sequencing techniques from patients suffering from developmental and epileptic encephalopathies (DEEs) (Melland et al. 2021). The three mutations were individually tested in SNAP-25 knockout mice that were rescued with wildtype or mutant SNAP-25B. All the three mutations result in substantially reduced eIPSC amplitudes and increased slopes; in other words, less Ca^{2+}-triggered neurotransmitter release and less synchrony (Alten et al. 2021).

More recent electrophysiological studies of synaptotagmin mutations of the primary interface suggest that the primary interface is essential for Ca^{2+}-evoked release, priming, and clamping of spontaneous release (Toulmé et al. 2024). Binding of synaptotagmin-1 C2B domain arginine residues to SNAP-25 acidic residues at one face of region II (Fig. 2.4) of the primary interface is crucial for Ca^{2+} triggering. In contrast, other SNAP-25 and syntaxin-1 acidic residues at region I (Fig. 2.4) of the primary interface are primarily involved in priming and clamping of spontaneous release. Importantly, the Glu295Ala mutation stabilizes the primary interface, but it reduces evoked release, suggesting that the wildtype primary interface is relatively dynamic and it sets the stage for the transition to a different state upon Ca^{2+} binding (see Sect. 2.9).

A hydrocarbon-stapled peptide, named SP9, was designed to disrupt Ca^{2+}-triggered membrane fusion by interfering with the primary interface (Lai et al.

2022). SP9 strongly suppressed Ca^{2+}-triggered fusion with reconstituted systems with neuronal synaptic proteins or their airway homologs (Brunger and Leitz 2023; Lai et al. 2022). Conjugation with the cell-penetrating peptide (CPP) penetratin (PEN) to the stapled peptide resulted in efficient delivery into cultured human airway epithelial cells and mouse airway epithelium, where it markedly and specifically reduced stimulated mucin secretion in both systems and substantially attenuated mucus occlusion of mouse airways. In contrast, SP9 did not affect baseline secretion in the IL-13 (metaplastic) cultures. Although SP9 is imperfect because it binds relatively weakly or variably to the synaptotagmin-1 C2B domain (Lai et al. 2022), it could serve as a therapeutic starting point as baseline mucin secretion is left unaffected, which is essential for maintaining the healthy state of airways.

A second interface, the so-called tripartite interface, was also observed by X-ray crystallography (Zhou et al. 2017), where the synaptotagmin-1 C2B domain binds to the SNARE–complexin-1 subcomplex via interactions with both the SNARE and complexin-1 components. However, thus far, the strongest support for the tripartite interface comes from electrophysiology experiments (Zhou et al. 2017) and molecular dynamics simulations (Brunger and Leitz 2023), but it has not yet been detected in solution (Jaczynska et al. 2023). Thus, further validation of the tripartite interface will be required. If the interface exists, it should ideally be visualized by cryo-ET reconstructions of docked/primed synaptic vesicles.

2.6 Tethering of Synaptic Vesicles by Munc13

Munc13-1 and its homologs are primarily brain-specific, cytoplasmic proteins in the presynaptic terminal involved in synaptic vesicle priming and short-term synaptic plasticity (Südhof 2012, 2013). In terms of domain structure, Munc13-1 consists of a C2 domain (C2A), a calmodulin-binding domain, a diacylglycerol (DAG)-binding C1 domain (C1), a Ca^{2+}/PIP2-binding C2 domain (C2B), the so-called MUN domain, and another C2 domain (C2C). The crystal structure of the C1C2BMUN fragment of Munc13-1 revealed interdomain interactions between the C1, C2B, and MUN domains and a folded linker region between the C1 and C2B domains (Xu et al. 2017). The C2A domain of Munc13-1 interacts with the Rab3 effector RIM, forming a tripartite complex (Dulubova et al. 2005), which is essential for the priming function of Munc13-1 and for the presynaptic localization in mice (Kaeser et al. 2011). RIM binding releases Munc13 from an autoinhibitory homodimer (Camacho et al. 2017; Deng et al. 2011), and genetic deletion of RIM reduces tethered synaptic vesicles (Fernández-Busnadiego et al. 2013).

Cryo-ET reconstructions of synapses (Fig. 2.2b, c) (Held et al. 2024a) and of synaptosomes (Orozco-Borunda et al. 2025; Papantoniou et al. 2023) suggest that Munc13-1 bridges synaptic vesicles to the plasma membrane via its C1C2B and C2C domains, as previously found (Camacho et al. 2021; Grushin et al. 2022; Quade et al. 2019) based on in vitro experiments. There are two different interaction modes of the C1C2B region with the plasma membrane: (i) one involving a polybasic face that is expected to yield an upright of Munc13-1 and hinder release and (ii)

another involving the DAG-Ca^{2+}-PIP2-binding face that is predicted to result in a lateral orientation and facilitate release (Camacho et al. 2021; Grushin et al. 2022). Indeed, the cryo-ET reconstructions of synapses (Held et al. 2024a) revealed roughly two different conformations of the tether densities in the tomograms of synapses (Fig. 2.2b, c) that are likely related to these two conformations of Munc13 when bridging synaptic vesicles and the plasma membrane.

2.7 Structural Biogenesis of *trans*-SNARE Complexes and Synaptic Vesicle Priming

This section focuses on how fusogenic *trans*-SNARE complexes (Fig. 2.1) are established.

2.7.1 Role of NSF

The AAA+ ATPase N-ethylmaleimide-sensitive factor (NSF, Sec18 in lower eukaryotes) and soluble NSF attachment proteins (SNAPs, Sec17 in lower eukaryotes) disassemble various SNARE complexes both before and after fusion (Huang et al. 2019; Khan et al. 2025; White et al. 2018, 2025; Zhao et al. 2015; Yousuf et al. 2021). Combined with functional studies with reconstituted systems (Lai et al. 2017; Ma et al. 2013; Stepien et al. 2019), NSF has also been established as a critical factor for synaptic vesicle priming before fusion. In particular, NSF and SNAP disassemble nonfusogenic SNARE complexes (White et al., 2025; Gao et al., 2023; Lai et al. 2017; Ma et al. 2013). Disassembly of off-pathway SNARE complexes allows neurons to recycle SNARE components locally and may act as a quality control mechanism for SNARE complex assembly. NSF and SNAP, along with an ATP regeneration system, improve the efficiency of subsequent Ca^{2+}-triggered fusion using a system with reconstituted components and isolated synaptic vesicles (Leitz et al. 2024a). Supporting the notion that NSF and SNAP disassemble nonfusogenic *cis*-SNARE complexes, several atomic-resolution cryo-EM structures were determined of NSF and SNAP in complex with the ternary neuronal SNARE complex (Huang et al. 2019; White et al. 2018; Zhao et al. 2015), a syntaxin tetramer, and two different binary complexes of syntaxin–SNAP-25 (White et al. 2025) (Fig. 2.5). All these complexes involve four-helix bundles of SNAREs, with the N-terminal end of one syntaxin or one SNAP-25 SNARE domain bound within the catalytic pore of the D1 ATPase hexamer of NSF.

What is the potential biological relevance of the syntaxin tetramer structure (Fig. 2.5a)? Syntaxin forms dense nanodomains at the active zone, and NSF directly colocalizes to these syntaxin clusters (Sieber et al. 2007; White et al. 2025). Thus, NSF and SNAP likely disassemble syntaxin tetramers and binary SNARE

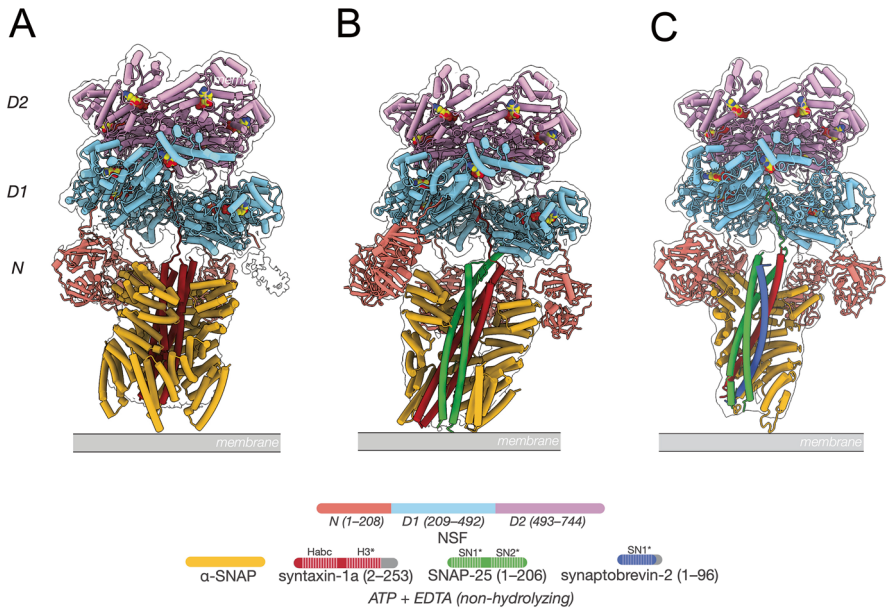


Fig. 2.5 (**a**) Hexameric NSF engages an α-SNAP–syntaxin tetramer subcomplex via its N-domains (salmon), several of which engage four α-SNAP molecules (gold) surrounding the soluble, tetrameric syntaxin H3 complex (dark red); the N-terminal end of one syntaxin is engaged in the D1 pore (light blue) (White et al. 2025). (**b**) Hexameric NSF engages the subcomplex consisting of α-SNAP and the 2:1 syntaxin–SNAP-25 (binary) SNARE complex via multiple N-domains (salmon), which engage three α-SNAP molecules (gold) surrounding the binary complex composed of two syntaxin H3 domains (dark red) and the SN1 and SN2 SNARE domains of a single SNAP-25 molecule (green). Part of the linker N-terminal to one of the syntaxin H3 domains is found within the catalytic D1 ring of NSF (light blue). (**c**) Hexameric NSF engages the subcomplex consisting of α-SNAP and the ternary SNARE complex. Hypothetical membranes are illustrated in gray. For the SNARE proteins, domains visible in the reconstruction of the SNARE complex are indicated with an asterisk

complexes on the perimeter of a given cluster to maintain a population of liberated syntaxin molecules. Munc18 can then capture individual syntaxin molecules liberated from clusters by NSF. Syntaxin nanodomains could thus effectively act as high-density storage sites for syntaxin, and NSF could tap these stores under periods of high-frequency vesicle release. It is also possible that NSF activity is regulated by post-translational modification (Gao et al. 2023; Zhou et al. 2013; Matveeva et al. 2001).

SNARE domains and TM regions introduce topological constraints for the disassembly process. Syntaxins are a particular case in point since they contain a large N-terminal (Habc) domain: a cryo-EM structure of a yeast SNARE complex, Sec18 (the NSF orthologue), and Sec17 (SNAP orthologue) in a nonhydrolyzing condition revealed that the SNARE Sso1 (the syntaxin-1A orthologue) is threaded through the D1 and D2 ATPase rings of Sec18, with its folded, N-terminal Habc domain

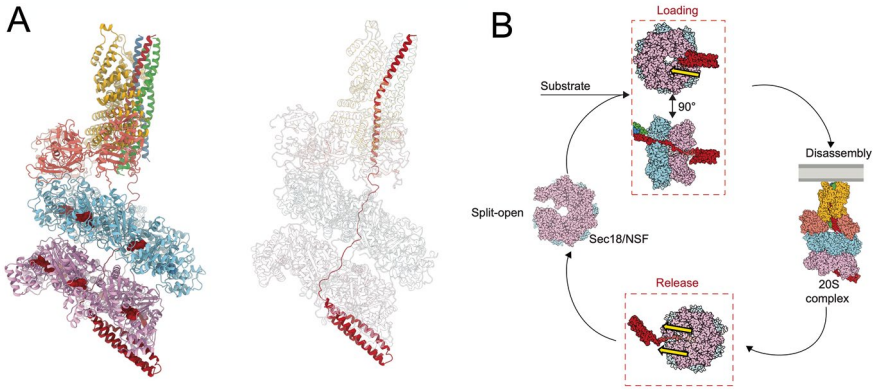


Fig. 2.6 (**a**) Sso1 (syntaxin homolog, dark red) is threaded through the D1 and D2 domains of Sec18 (NSF homolog). The N-terminal (Habc) domain of Sso1 interacts with the D2 ATPase ring of Sec18 (Khan et al. 2025). Left subpanel: cartoon representation of the complex of the yeast SNARE complex (consisting of Sso1, Snc1 (light blue), and Sec9 (green)), Sec18 (salmon, light blue, pink), and Sec17 (α-SNAP homolog, gold). Right subpanel: All parts are shown at high transparency except for Sso1. (**b**) Mechanism of substrate side-loading and side-release for Sec18/NSF

interacting with the D2 ring (Fig. 2.6) (Khan et al. 2025). Moreover, the N-terminal domain of syntaxin does not unfold during Sec18/NSF activity, as shown with single-molecule FRET experiments with NSF. Cryo-EM structures under hydrolyzing conditions revealed substrate-released and substrate-free states of Sec18 with a coordinated opening in the side of the ATPase rings. These findings suggest that Sec18/NSF can operate by substrate side-loading and unloading topologically constrained SNARE substrates. Sec18/NSF can load and release SNARE substrates via a coordinated opening in the D1 and D2 rings. This mechanism does not preclude the more conventional notion of complete substrate threading through the pores of Sec18/NSF if the SNARE substrate is not topologically restricted by membrane domains or anchors or by N-terminal domains or complexes.

How does NSF recognize SNARE substrates? Considering that we observe either syntaxin or SNAP-25 to be bound to the D1 pore (Khan et al. 2025; White et al. 2018, 2025), as well as part of the N-terminal domain in a self-inhibiting state of NSF (Khan et al. 2025), the interaction with D1 is likely highly promiscuous. The specificity of SNARE substrates is, therefore, likely conferred by the interactions between SNAP molecules and SNAREs, and these interactions are primarily driven by charge–charge complementarity (White et al. 2018). Consequently, complexin-1 and/or synaptotagmin-1 binding is expected to interfere with some SNAP–SNARE interactions. Indeed, complexin inhibits NSF-mediated disassembly of neuronal SNARE complexes in a dose-dependent fashion (Choi et al. 2018).

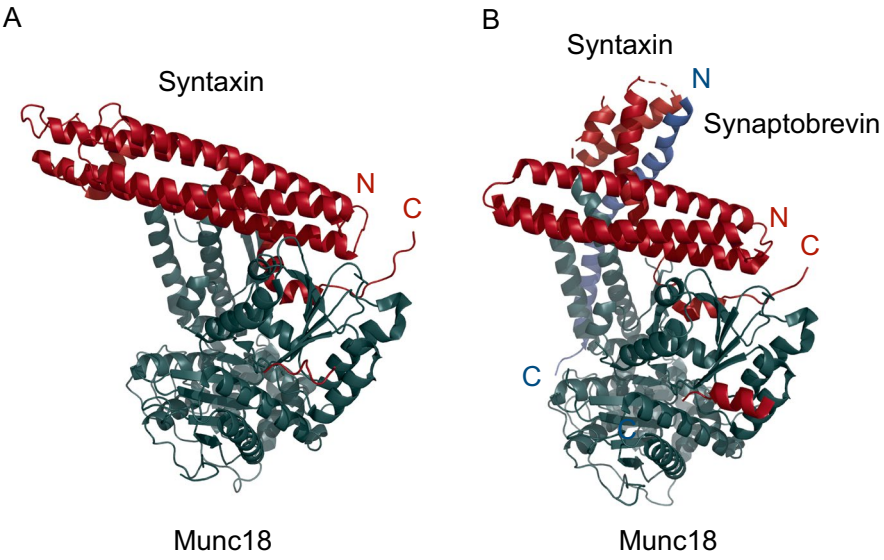


Fig. 2.7 (**a**) Crystal structure of the syntaxin-1a (dark red)–Munc18a (dark teal) complex (Burkhardt et al. 2008; Misura et al. 2000). (**b**) Cryo-EM structure of the synaptobrevin (light blue)–Munc18-1 (dark teal)–syntaxin-1 (dark red) complex (Stepien et al. 2022). The N- and C-terminal ends of the visible fragments of syntaxin and synaptobrevin are labeled

2.7.2 Role of Munc18 and Munc13

The activity of NSF establishes syntaxin–Munc18 complexes (Fig. 2.7a) that can be considered the starting point for synaptic vesicle priming. The MUN domain of Munc13-1 catalyzes the transit of syntaxin-1A from the syntaxin-1A–Munc18-1 complex into the ternary *trans-SNARE* complex (Basu et al. 2005; Ma et al. 2013; Yang et al. 2015) and promotes the proper assembly of the SNARE complex (Lai et al. 2017). Before the action of Munc13, Munc18 forms a scaffolding complex with the cytoplasmic regions of synaptobrevin and syntaxin (Stepien et al. 2022) (Fig. 2.7b). This complex positions the C-terminal ends of the cytoplasmic regions of synaptobrevin and syntaxin, such that they could reach the synaptic vesicle and plasma membranes, respectively. This complex would initiate interactions between synaptobrevin and syntaxin that lead to the *trans*-SNARE complex formation through the action of Munc13 which changes the conformation of syntaxin and allows the SNARE domain of syntaxin to interact with synaptobrevin and SNAP-25. Synaptotagmin-1 then binds to the assembled *trans*-SNARE complex via the primary interface (Zhou et al. 2015), and complexin-1 also binds to the *trans*-SNARE complex (Chen et al. 2002).

When the soluble fragments of SNARE proteins are simply mixed in solution, improper configurations may occur (Choi et al. 2016; Lou et al. 2015; Ryu et al. 2015; Weninger et al. 2003). In particular, nonfunctional antiparallel SNARE

complex configurations were observed using single-molecule fluorescence resonance energy transfer (FRET) experiments (Choi et al. 2016; Weninger et al. 2003). Thus, the assembly of a functional SNARE complex is an active process, and the ancillary proteins involved in the assembly (and disassembly) of the SNARE complex are crucial to sustained neuron function.

2.8 Dynamic Character of Docked Synaptic/Primed Synaptic Vesicles

The ability to capture membrane-proximal synaptic vesicles in electron microscopy/cryo-ET reconstructions of resting neurons gives the impression of a relatively static state. However, flash freeze and simulation experiments suggested that vesicle docking and priming are dynamic and may be reversible (Kusick et al. 2022; Murthy and Stevens 1999; Neher and Brose 2018; Silva et al. 2021). In support of this notion, dissociation of previously docked synaptic vesicles was observed in a reconstituted system with isolated synaptic vesicles, plasma membrane-mimicking vesicles, NSF, α-SNAP, Munc13, and Munc18 (Leitz et al. 2024a). It is likely that the membrane-bridging/tethering activity by the C1C2BMUNC2C fragment of Munc13 (Camacho et al. 2021; Grushin et al. 2022) (Fig. 2.2b, c) physically permits the exchange and clearance of α-SNAP from the synaptic vesicle–plasma membrane interface. In addition, the presence of the C1, C2B, and C2C domains effectively increases the local concentration of Munc13 near the synaptic vesicle docking site. The lateral conformation of C1C2BMUNC2C (Camacho et al. 2021; Grushin et al. 2022; Quade et al. 2019) brings the synaptic vesicle closer to the plasma membrane (compare Fig. 2.2b and c). Munc18 and Munc13 act together (Prinslow et al. 2019; Stepien et al. 2019), domain 3a of Munc18 interacts with the full-length assembled SNARE complex (Parisotto et al. 2014), and Munc13 interacts directly with synaptobrevin and SNAP-25 during addition to the SNARE complex to ensure parallel SNARE complex formation (Kalyana Sundaram et al. 2021; Lai et al. 2017; Shu et al. 2020; Wang et al. 2019). Thus, these processes likely promote the formation of the primed SNARE–synaptotagmin-1–complexin-1 prefusion complex (Fig. 2.4) (Zhou et al. 2015, 2017) and protect the *trans*-SNARE complex from α-SNAP binding and disassembly (Choi et al. 2018). In contrast, improperly or incompletely formed SNARE complexes may not efficiently bind complexin-1 and synaptotagmin-1, consequently enabling α-SNAP binding for subsequent disassembly by NSF and effectively inhibiting any fusion activity by these complexes. In support of this notion, there is an increase in spontaneous fusion when the ATP concentration is not maintained in a reconstituted system (Leitz et al. 2024a).

2.9 Models of Ca^{2+} Triggering of Synaptic Vesicles

The SNARE complex provides the energy necessary for membrane fusion (Sutton et al. 1998; Weber et al. 1998). During fusion, the *trans*-SNARE complex completely zippers into the fully assembled *cis*-SNARE complex, where the soluble core consists of a parallel, four-α-helix bundle. At least two synaptobrevin-2 molecules, and presumably two SNARE complexes, are required for fast Ca^{2+}-triggered exocytosis (Sinha et al. 2011). However, binding to synaptotagmin-1 and complexin-1 arrests the *trans*-SNARE complex, so it cannot promote fusion at resting Ca^{2+} concentration (Voleti et al. 2020; Zhou et al. 2015). The synaptotagmin-1 C2B domain contains many charged residues consisting of clusters of basic residues on the surface of the β-sandwich, including the so-called polybasic region, which can interact with anionic membranes (Pérez-Lara et al. 2016; Voleti et al. 2020). These membrane interactions enhance the primary interface at resting Ca^{2+} concentration by simultaneously binding the polybasic region and the SNARE complex to the membrane (Grushin et al. 2019; Voleti et al. 2020; Zhou et al. 2015).

Upon Ca^{2+} binding to the C2 domains of synaptotagmin, the inhibition is released, and fusion is triggered on a fast time scale. Several models have been proposed for the release of this inhibition: (1) The synaptotagmin C2B molecule that forms the primary interface induces membrane puckering in conjunction with the SNARE complex upon Ca^{2+} binding of the membrane near the fusion site (Zhou et al. 2015) (Fig. 2.8a). (2) Ca^{2+} triggering of synaptic vesicle fusion causes a rearrangement of the primary interface involving dissociation of region I, while region II remains bound (Jaczynska et al. 2025; Toulmé et al. 2024). This rearrangement may act as a

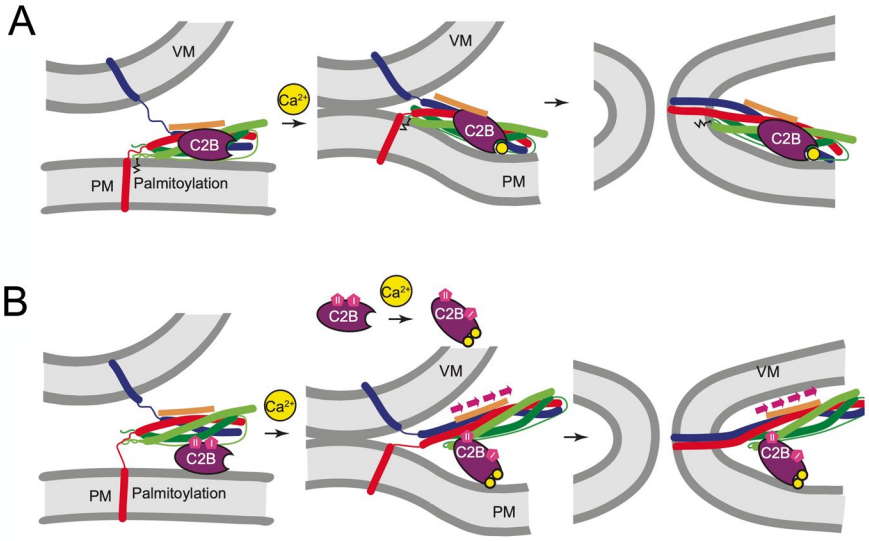


Fig. 2.8 Models of Ca^{2+} triggering. (**a**) Membrane bending model proposed in reference Zhou et al. (2015). (**b**) Pivot model (Toulmé et al. 2024). VM: vesicle membrane, PM: vesicle membrane

lever that pulls the SNARE complex when Ca^{2+} causes reorientation of the C2B domain, facilitating zippering and membrane fusion (Fig. 2.8b). (3) The complexin-1 accessory helix inhibits release through electrostatic (and perhaps steric) repulsion of the synaptic vesicle by its location between the vesicle and plasma membranes (Rizo 2022; Trimbuch et al. 2014). (4) If the tripartite interface between a second synaptotagmin-1 C2B domain and SNARE–complexin subcomplex exists, it may dislodge upon Ca^{2+} binding, further enhancing the effect of the C2B domain that is initially bound to the primary interface (Zhou et al. 2017). Finally, several of these mechanisms may act together. Further studies will be needed to clarify the Ca^{2+}-triggering mechanism.

2.10 New Insights into the Biogenesis of Synaptic Vesicles

Before docking and priming, synaptic vesicles are formed, primarily through clathrin-mediated endocytosis (Heuser and Reese 1973; Maycox et al. 1992; Watanabe et al. 2014). Synaptic vesicles have a remarkably well-defined proteome and copy number distribution (Takamori et al. 2006). Interaction maps of synaptic vesicle proteins have been obtained based on cross-linking mass spectrometry (Wittig et al. 2021), although the structural details are unclear. As a first step to decipher the molecular architecture of synaptic vesicles, glutamatergic ISVs were

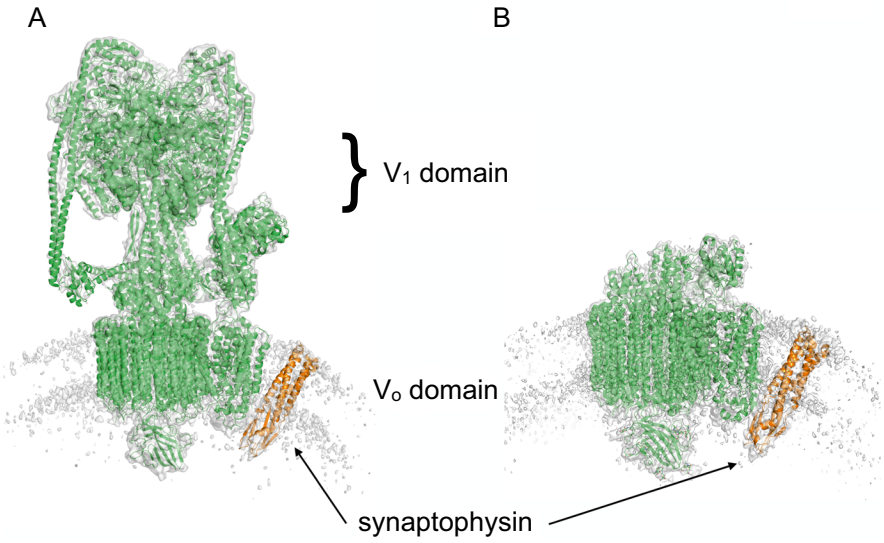


Fig. 2.9 (**a**) In situ structures of the V-ATPase (PDB ID 9BRQ) and (**b**) V0-only V-ATPase (PDB ID 9BRZ) assembly in synaptic vesicle membranes (Wang et al. 2024). V-ATPase is colored green, and synaptophysin is colored orange. The EM density maps (gray) are superimposed. The gray arc represents the ISV membrane density

immuno-isolated and purified from mouse brains and imaged by cryo-EM and cryo-ET (Leitz et al. 2024a, b; Takamori et al. 2006). The ISVs were functional as assessed by a Ca^{2+}-triggered vesicle–vesicle fusion assay (Leitz et al. 2024a).

In situ structures of V-ATPases in functional, glutamatergic mouse ISVs were obtained by subtomogram averaging of cryo-ET data and by reconstructions with single-particle mode cryo-EM data (Wang et al. 2024) (Fig. 2.9). Both intact and V0-only V-ATPase assemblies were observed, consistent with the observation that V-ATPases reversibly dissociate the V1 domain upon synaptic vesicle acidification (Bodzęta et al. 2017). The cryo-ET and cryo-EM structures revealed that synaptophysin is bound to the synaptic vesicle V-ATPase (Wang et al. 2024). Two other research groups independently observed a similar interaction at similar resolutions (Coupland et al. 2024; Kravcenko et al. 2024). Considering the limited resolution of these reconstructions and to further confirm the identity of the binding partner, synaptophysin knockout ($Syp^{-/-}$) mice were used (Wang et al. 2024), and the resulting

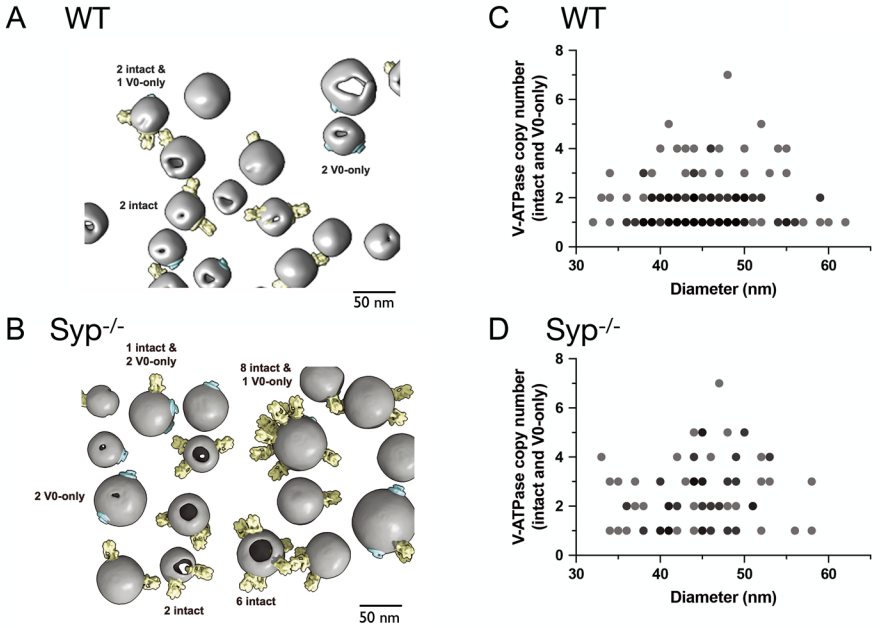


Fig. 2.10 Renderings of representative tomographic reconstructions of isolated synaptic vesicles from (**a**) wildtype (WT) and (**b**) $Syp^{-/-}$ mouse brains. The synaptic vesicle membrane, the intact, and V0-only V-ATPase assemblies are colored in gray, yellow, and cyan, respectively. (**c**, **d**) Scatter plots of the ISV diameters and V-ATPase copy numbers (including both intact and V0-only assemblies) for wildtype (**c**) and $Syp^{-/-}$ ISVs (**d**) from six randomly selected tomograms, respectively. The gray scale of the dots indicates the number of cases (dark: more frequent cases). The simple linear regression *p*-value (analyzed by GraphPad Prism V.10) between the WT and $Syp^{-/-}$ datasets is 0.56 and 0.08, respectively, indicating no statistically significant correlation between ISV diameters and V-ATPase copy numbers. (The source data are associated with Extended Data Fig. 8i in reference Wang et al. (2024))

cryo-EM maps revealed the absence of a binding partner to V-ATPase in the Syp$^{-/-}$ ISVs, thus confirming the identity of the binding partner to wildtype synaptic vesicle V-ATPases. Considering that synaptoporin and synaptogyrin (close homologs of synaptophysin) are present in the Syp$^{-/-}$ mice (Wang et al. 2024), the interaction between V-ATPase and synaptophysin is, therefore, highly specific to synaptophysin.

The copy number of V-ATPases roughly doubled in Syp$^{-/-}$ ISVs compared to wildtype ISVs (Wang et al. 2024) (Fig. 2.10). The size distributions of the ISVs are similar, and there is no correlation between the V-ATPase copy numbers and ISV diameters for both wildtype and Syp$^{-/-}$ ISVs; in other words, the average ISV diameter is similar (Wang et al. 2024) (Fig. 2.10c, d). However, in synaptophysin/synaptoporin/synaptogyrin-1/synaptogryin-3 quadruple knockout mice, the diameter of synaptic vesicles is substantially increased (Park et al. 2024), suggesting that the loss of synaptophysin in Syp$^{-/-}$ mice is partially compensated by the presence of the other members of the synaptophysin family in determining the synaptic vesicle size. A possible explanation for the increased copy number of V-ATPases in Syp$^{-/-}$ ISVs is that the absence of the V-ATPase–synaptophysin interaction effectively decreases the lateral membrane cross section of the combined molecular assembly. This smaller membrane cross section will reduce molecular crowding by decreasing the excluded surface area (Ellis 2001), resulting in a higher V-ATPase copy number in Syp$^{-/-}$ ISVs. However, the effect of a single synaptophysin molecule interacting with the V-ATPase may not be large enough to explain the roughly twofold effect on the V-ATPase copy number (Wang et al. 2024). It is possible, or even likely, that synaptophysin is also involved in interactions with synaptobrevin (Adams et al. 2015), and synaptophysin itself can form oligomers (Arthur and Stowell 2007; Bera et al. 2023). These additional interactions would then effectively increase the cross section of this supramolecular complex. However, these additional interactions with synaptophysin have not yet been observed in cryo-ET/cryo-EM studies of synaptic vesicles, possibly due to heterogeneity. In any case, we speculate that the interactions involving the synaptophysin family of proteins play a fundamental role in synaptic vesicle biogenesis.

At the gross morphological level, Syp$^{-/-}$ mice form normal synapses and synaptic vesicles (Eshkind and Leube 1995), corroborated by the cryo-ET reconstructions of Syp$^{-/-}$ ISVs (Wang et al. 2024). Syp$^{-/-}$ mice exhibit normal EPSC and mEPSC release probabilities, though a small but significant increase in EPSC quantal amplitude was previously observed (McMahon et al. 1996). More profound changes were observed with double genetic deletion of both synaptophysin and synaptogyrin, reducing short-term and long-term plasticity in neurons (Janz et al. 1999). Quadruple knockout studies of the entire brain-enriched synaptophysin family (synaptophysin/synaptoporin/synaptogyrin-1/synaptogryin-3) produced an even more significant increase in quantal amplitude (Raja et al. 2019). Importantly, Syp$^{-/-}$ mice exhibit a severe seizure phenotype under pharmacological treatment with a glutamate agonist (Wang et al. 2024), concordant with the increase in quantal size observed for both

Syp$^{-/-}$ and quadruple knockout (McMahon et al. 1996; Raja et al. 2019). The increased V-ATPase copy number in Syp$^{-/-}$ ISVs offers a possible explanation for the observed seizure phenotype, concordant with the increase in quantal size observed in previous Syp$^{-/-}$ knockout studies (McMahon et al. 1996; Raja et al. 2019). The increased quantal size could be different in excitatory and inhibitory synapses, as suggested by different synaptophysin copy numbers in glutamatergic and GABAergic wildtype ISVs (Grønborg et al. 2010).

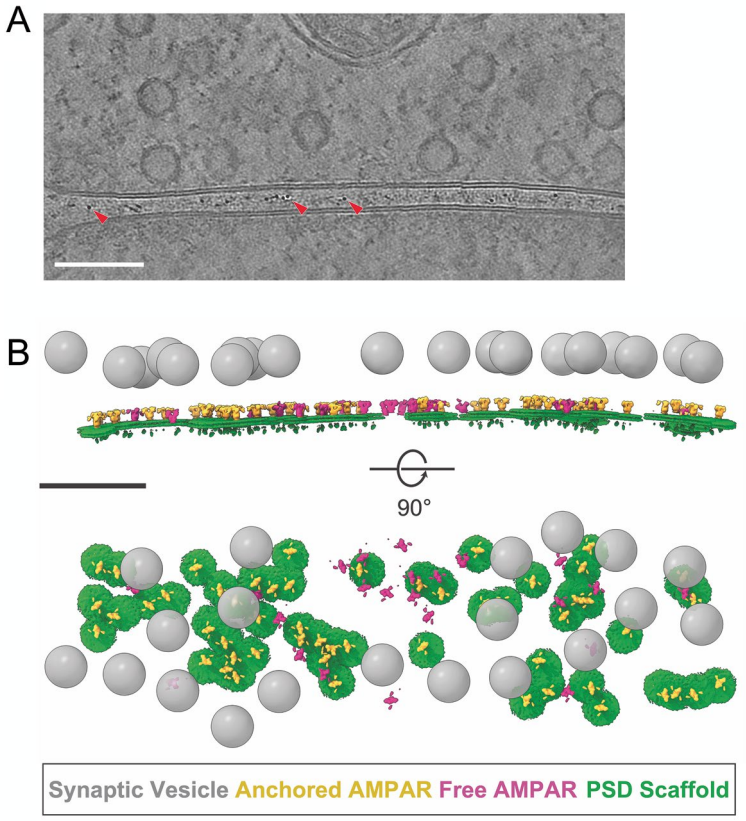


Fig. 2.11 (**a**) Slice (1 nm thick) through a 3D cryo-ET reconstruction of a synapse (1 nm/pixel). Scale bar: 100 nm. Red arrows indicate selected Au-NP positions. (**b**) Representative AMPAR-ECD (yellow and magenta) and PSD (green) sub-tomogram average maps back-plotted to their tomogram positions and displayed along with membrane-proximal synaptic vesicles (gray (Held et al. 2024b)). AMPARs engaged with PSD scaffolds are colored yellow, whereas un-anchored AMPARs are colored magenta (Held et al. 2024b)

2.11 New Insights into the Nanotopography of Synapses

Although docking presynaptic proteins and their complexes into densities is compelling (Fig. 2.2b–d), subtomogram averaging will be required to confirm the identity of the observed densities. Moreover, most observed densities will likely require labeling or genetic knockout approaches for identification. As a first step to establish the utility of labeling, endogenously expressed AMPA receptors were labeled with gold nanoparticles (AuNPs) using SpyCatcher/Tag and mapped the molecular topography of AMPARs mapped with cryo-ET reconstructions, relating receptor localizations to synapse ultrastructure in near-native conditions (Held et al. 2024b) (Fig. 2.11a).

Supramolecular clusters of active zone and postsynaptic density scaffolds were observed on the scale of tens of nanometers and trans-synaptic alignment of said nanoclusters into nanocolumns (Held et al. 2024a, b), consistent with previous studies using super-resolution fluorescence microscopy (MacGillavry et al. 2013; Nair et al. 2013; Sakamoto et al. 2018; Tang et al. 2016) and cryo-ET studies of unlabeled synaptosomes (Martinez-Sanchez et al. 2021). However, in the studies of intact synapses, membrane-proximal synaptic vesicles are mostly offset from AMPAR nanoclusters and trans-synaptic scaffold nanocolumns (Held et al. 2024a, b) (Fig. 2.11b). Thus, synaptic vesicles are not preferentially aligned with nanocolumns, although there are a very small number of membrane-proximal (membrane–membrane distance less than 10 nm) synaptic vesicles aligned with AMPARs.

What could be the mechanism for these offsets? Active zone nanoclusters may act at an upstream step to capture synaptic vesicles and allow the formation of initial membrane tethering interactions by Munc13 (Quade et al. 2019). These synaptic vesicles could then disperse from active zone nanoclusters and proceed with priming processes. While the resulting offset of synaptic vesicles may only amount to shifts of tens of nanometers, such distances can potentially impact downstream signal transduction (Eggermann et al. 2012; Raghavachari and Lisman 2004).

What is the consequence of these spatial offsets between synaptic vesicles and AMPAR nanoclusters? It is tempting to speculate that these offsets are related to different forms of synaptic vesicle fusion. Synaptic vesicles fuse both synchronously and asynchronously in response to action potentials (Südhof 2013), and fusion sites for both types of release are likely spatially segregated (Li et al. 2021; Malagon et al. 2023). Additionally, spontaneous release probably occurs at distinct release sites (Wang et al. 2022b) that could be spatially separated from evoked release sites. Moreover, the lateral offsets between AMPAR nanoclusters and membrane-proximal synaptic vesicles likely determine synaptic strength and plasticity. Monte Carlo simulations based on tomographic reconstructions suggest that offsets between synaptic vesicles and nano-clustered AMPARs introduce larger variability in postsynaptic response amplitude than expected if AMPARs were randomly distributed throughout the synapse (Held et al. 2024a), as had been observed in electrophysiological recordings of hippocampal neurons many years ago (Bekkers

et al. 1990). Further studies are needed since the present cryo-ET reconstructions do not allow one to infer the vesicular release probability of membrane-proximal synaptic vesicles.

2.12 Conclusions

The recent results presented in this chapter illustrate the potential of in situ cryo-EM/cryo-ET imaging methods for discovering new interactions or uncovering the molecular details of a known interaction. We foresee rich opportunities to pursue other proteins and their complexes in the synapse and to visualize the predominant information transfer path in the nervous system at a molecular level. Such knowledge of the spatial organization of the synapse will provide a framework for a deeper understanding of the molecular mechanisms that underlie neuronal communication.

Acknowledgments We thank Josep Rizo, Liv Jensen, Paul Lapios, and Vladan Lučić for stimulating discussions and Vladan Lučić for providing the cryo-ET maps shown in Fig. 2.3. Funding was provided by the US National Institutes of Health (NIH; RO1MH63105 to A.T.B.). This chapter is subject to HHMI's Open Access to Publications policy. HHMI laboratory heads have previously granted a non-exclusive CC BY 4.0 license to the public and a sublicensable license to HHMI in their research articles. Pursuant to those licenses, the author-accepted manuscript of this chapter can be made freely available under a CC BY 4.0 license immediately upon publication.

References

Adams DJ, Arthur CP, Stowell MHB. Architecture of the synaptophysin/synaptobrevin complex: structural evidence for an entropic clustering function at the synapse. Sci Rep. 2015;5(1):13659.

Aeffner S, Reusch T, Weinhausen B, Salditt T. Energetics of stalk intermediates in membrane fusion are controlled by lipid composition. Proc Natl Acad Sci USA. 2012;109(25):E1609–18.

Alten B, Zhou Q, Shin OH, Esquivies L, Lin PY, White KI, et al. Role of aberrant spontaneous neurotransmission in SNAP25-associated encephalopathies. Neuron. 2021;109(1):59–72.e5.

Arthur CP, Stowell MHB. Structure of synaptophysin: a hexameric MARVEL-domain channel protein. Struct Lond Engl 1993. 2007;15(6):707–14.

Basu J, Shen N, Dulubova I, Lu J, Guan R, Guryev O, et al. A minimal domain responsible for Munc13 activity. Nat Struct Mol Biol. 2005;12(11):1017–8.

Bekkers JM, Richerson GB, Stevens CF. Origin of variability in quantal size in cultured hippocampal neurons and hippocampal slices. Proc Natl Acad Sci USA. 1990;87(14):5359–62.

Bera M, Radhakrishnan A, Coleman JK, Sundaram RV, Ramakrishnan S, Pincet F, et al. Synaptophysin chaperones the assembly of 12 SNAREpins under each ready-release vesicle. Proc Natl Acad Sci USA [Internet]. 2023;120(45):e2311484120. Available from: https://pnas.org/doi/10.1073/pnas.2311484120.

Bodzęta A, Kahms M, Klingauf J. The presynaptic v-ATPase reversibly disassembles and thereby modulates exocytosis but is not part of the fusion machinery. Cell Rep. 2017;20(6):1348–59.

Brunger AT, Leitz J. The core complex of the Ca2+-triggered presynaptic fusion machinery. J Mol Biol. 2023;435(1):167853.

Brunger AT, Choi UB, Lai Y, Leitz J, Zhou Q. Molecular mechanisms of fast neurotransmitter release. Annu Rev Biophys. 2018;47(1):469–97.

Buchholz TO, Jordan M, Pigino G, Jug F. Cryo-CARE: content-aware image restoration for cryo-transmission electron microscopy data. In: 2019 IEEE 16th international symposium on biomedical imaging (ISBI 2019). IEEE; 2018. p. 1–5.

Burkhardt P, Hattendorf DA, Weis WI, Fasshauer D. Munc18a controls SNARE assembly through its interaction with the syntaxin N-peptide. EMBO J. 2008;27(7):923–33.

Camacho M, Basu J, Trimbuch T, Chang S, Pulido-Lozano C, Chang SS, et al. Heterodimerization of Munc13 C2A domain with RIM regulates synaptic vesicle docking and priming. Nat Commun. 2017;8(1):15293.

Camacho M, Quade B, Trimbuch T, Xu J, Sari L, Rizo J, et al. Control of neurotransmitter release by two distinct membrane-binding faces of the Munc13-1 C1C2B region. elife. 2021;10:1–34.

Chen X, Tomchick DR, Kovrigin E, Araç D, Machius M, Südhof TC, et al. Three-dimensional structure of the complexin/SNARE complex. Neuron. 2002;33(3):397–409.

Choi UB, Zhao M, Zhang Y, Lai Y, Brunger AT. Complexin induces a conformational change at the membrane-proximal C-terminal end of the SNARE complex. elife. 2016;5(9):e16886.

Choi UB, Zhao M, White KI, Pfuetzner RA, Esquivies L, Zhou Q, et al. NSF-mediated disassembly of on- and off-pathway SNARE complexes and inhibition by complexin. elife [Internet]. 2018;7:e36497. Available from: https://elifesciences.org/articles/36497.

Coupland CE, Karimi R, Bueler SA, Liang Y, Courbon GM, Di Trani JM, et al. High-resolution electron cryomicroscopy of V-ATPase in native synaptic vesicles. Science. 2024;385(6705):168–74.

Deng L, Kaeser PS, Xu W, Südhof TC. RIM proteins activate vesicle priming by reversing autoinhibitory homodimerization of Munc13. Neuron. 2011;69(2):317–31.

Denker A, Kröhnert K, Bückers J, Neher E, Rizzoli SO. The reserve pool of synaptic vesicles acts as a buffer for proteins involved in synaptic vesicle recycling. Proc Natl Acad Sci USA. 2011;108(41):17183–8.

Dulubova I, Lou X, Lu J, Huryeva I, Alam A, Schneggenburger R, et al. A Munc13/RIM/Rab3 tripartite complex: from priming to plasticity? EMBO J. 2005;24(16):2839–50.

Eggermann E, Bucurenciu I, Goswami SP, Jonas P. Nanodomain coupling between Ca2+ channels and sensors of exocytosis at fast mammalian synapses. Nat Rev Neurosci. 2012;13(1):7–21.

Ellis RJ. Macromolecular crowding: obvious but underappreciated. Trends Biochem Sci. 2001;26(10):597–604.

Eshkind LG, Leube RE. Mice lacking synaptophysin reproduce and form typical synaptic vesicles. Cell Tissue Res. 1995;282(3):423–33.

Fernández-Busnadiego R, Asano S, Oprisoreanu AM, Sakata E, Doengi M, Kochovski Z, et al. Cryo-electron tomography reveals a critical role of RIM1 α in synaptic vesicle tethering. J Cell Biol. 2013;201(5):725–40.

Gao Y, Khan YA, Mo W, White KI, Perkins M, Pfuetzner RA, et al. Sensory deficit screen identifies nsf mutation that differentially affects SNARE recycling and quality control. Cell Rep. 2023;42(4):112345.

Gipson P, Fukuda Y, Danev R, Lai Y, Chen DH, Baumeister W, et al. Morphologies of synaptic protein membrane fusion interfaces. Proc Natl Acad Sci USA. 2017;114(34):9110–5.

Grønborg M, Pavlos NJ, Brunk I, Chua JJE, Münster-Wandowski A, Riedel D, et al. Quantitative comparison of glutamatergic and GABAergic synaptic vesicles unveils selectivity for few proteins including MAL2, a novel synaptic vesicle protein. J Neurosci. 2010;30(1):2–12.

Grushin K, Wang J, Coleman J, Rothman JE, Sindelar CV, Krishnakumar SS. Structural basis for the clamping and Ca2+ activation of SNARE-mediated fusion by synaptotagmin. Nat Commun. 2019;10(1):1–12.

Grushin K, Kalyana Sundaram RV, Sindelar CV, Rothman JE. Munc13 structural transitions and oligomers that may choreograph successive stages in vesicle priming for neurotransmitter release. Proc Natl Acad Sci USA [Internet]. 2022;119(7):e2121259119. Available from: https://pnas.org/doi/full/10.1073/pnas.2121259119.

Held RG, Kaeser PS. ELKS active zone proteins as multitasking scaffolds for secretion. Open Biol. 2018;8(2):170258.

Held RG, Liang J, Brunger AT. Nanoscale architecture of synaptic vesicles and scaffolding complexes revealed by cryo-electron tomography. Proc Natl Acad Sci USA [Internet]. 2024a;121(27):e2403136121. Available from: https://pnas.org/doi/10.1073/pnas.2403136121.

Held RG, Liang J, Esquivies L, Khan YA, Wang C, Azubel M, et al. In-situ structure and topography of AMPA receptor scaffolding complexes visualized by cryoET. bioRxiv. 2024b. https://doi.org/10.1101/2024.10.19.619226.

Heuser JE, Reese TS. Evidence for recycling of synaptic vesicle membrane during transmitter release at the frog neuromuscular junction. J Cell Biol. 1973;57(2):315–44.

Huang X, Sun S, Wang X, Fan F, Zhou Q, Lu S, et al. Mechanistic insights into the SNARE complex disassembly. Sci Adv. 2019;5(4):eaau8164.

Imig C, Min SW, Krinner S, Arancillo M, Rosenmund C, Südhof TC, et al. The morphological and molecular nature of synaptic vesicle priming at presynaptic active zones. Neuron. 2014;84(2):416–31.

Jaczynska K, Esquivies L, Pfuetzner RA, Alten B, Brewer KD, Zhou Q, et al. Analysis of tripartite synaptotagmin-1-SNARE-complexin-1 complexes in solution. FEBS Open Bio. 2023;13:26–50.

Jaczynska K, Esser V, Xu J, Sari L, Lin MM, Rosenmund C, et al. A lever hypothesis for synaptotagmin-1 action in neurotransmitter release. Proc Natl Acad Sci USA. 2025;122(1):e2417941121.

Janz R, Südhof TC, Hammer RE, Unni V, Siegelbaum SA, Bolshakov VY. Essential roles in synaptic plasticity for synaptogyrin I and synaptophysin I. Neuron. 1999;24(3):687–700.

Kaeser PS, Deng L, Wang Y, Dulubova I, Liu X, Rizo J, et al. RIM proteins tether Ca2+ channels to presynaptic active zones via a direct PDZ-domain interaction. Cell. 2011;144(2):282–95.

Kalyana Sundaram RV, Jin H, Li F, Shu T, Coleman J, Yang J, et al. Munc13 binds and recruits SNAP25 to chaperone SNARE complex assembly. FEBS Lett. 2021;595(3):297–309.

Khan YA, White KI, Pfuetzner RA, Singal B, Esquivies L, Mckenzie G, et al. SNARE disassembly requires Sec18/NSF side loading. Nat Struct Mol Biol. 2025;32:1708-1720. Nature Structural & Molecular Biology. 2025; 32:1708–20.

Korogod N, Petersen CC, Knott GW. Ultrastructural analysis of adult mouse neocortex comparing aldehyde perfusion with cryo fixation. elife. 2015;4:e05793.

Kravcenko U, Ruwolt M, Kroll J, Yushkevich A, Zenkner M, Ruta J, et al. Molecular architecture of synaptic vesicles. bioRxiv. 2024. https://doi.org/10.1101/2024.04.11.588828.

Kusick GF, Ogunmowo TH, Watanabe S. Transient docking of synaptic vesicles: implications and mechanisms. Curr Opin Neurobiol. 2022;74:102535.

Lai Y, Choi UB, Leitz J, Rhee HJ, Lee C, Altas B, et al. Molecular mechanisms of synaptic vesicle priming by Munc13 and Munc18. Neuron. 2017;95(3):591–607.e10.

Lai Y, Fois G, Flores JR, Tuvim MJ, Zhou Q, Yang K, et al. Inhibition of calcium-triggered secretion by hydrocarbon-stapled peptides. Nature. 2022;603(7903):949–56.

Leitz J, Wang C, Esquivies L, Pfuetzner RA, Peters JJ, Couoh-Cardel S, et al. Beyond the MUN domain, Munc13 controls priming and depriming of synaptic vesicles. Cell Rep. 2024a;43(5):114026.

Leitz J, Wang C, Esquivies L, Peters JJ, Gopal N, Pfuetzner RA, et al. Observing isolated synaptic vesicle association and fusion ex vivo. Nat Protoc [Internet]. 2024b;19:3139–61. Available from: https://www.nature.com/articles/s41596-024-01014-x.

Li S, Raychaudhuri S, Lee SA, Brockmann MM, Wang J, Kusick G, et al. Asynchronous release sites align with NMDA receptors in mouse hippocampal synapses. Nat Commun. 2021;12(1):677.

Lin KH, Taschenberger H, Neher E. A sequential two-step priming scheme reproduces diversity in synaptic strength and short-term plasticity. Proc Natl Acad Sci USA. 2022;119(34):e2207987119.

Lou X, Shin J, Yang Y, Kim J, Shin YK. Synaptotagmin-1 is an antagonist for Munc18-1 in SNARE zippering. J Biol Chem. 2015;290:10535.

Lučić V, Fernández-Busnadiego R, Laugks U, Baumeister W. Hierarchical detection and analysis of macromolecular complexes in cryo-electron tomograms using Pyto software. J Struct Biol. 2016;196(3):503–14.

Ma C, Su L, Seven AB, Xu Y, Rizo J. Reconstitution of the vital functions of Munc18 and Munc13 in neurotransmitter release. Science. 2013;339(6118):421–5.

MacGillavry HD, Song Y, Raghavachari S, Blanpied TA. Nanoscale scaffolding domains within the postsynaptic density concentrate synaptic AMPA receptors. Neuron. 2013;78(4):615–22.

Malagon G, Myeong J, Klyachko VA. Two forms of asynchronous release with distinctive spatio-temporal dynamics in central synapses. elife. 2023;12:e84041.

Martinez-Sanchez A, Laugks U, Kochovski Z, Papantoniou C, Zinzula L, Baumeister W, et al. Trans-synaptic assemblies link synaptic vesicles and neuroreceptors. Sci Adv. 2021;7:eabe6204.

Maycox PR, Link E, Reetz A, Morris SA, Jahn R. Clathrin-coated vesicles in nervous tissue are involved primarily in synaptic vesicle recycling. J Cell Biol. 1992;118(6):1379–88.

Matveeva EA, Whiteheart SW, Vanaman TC, & Slevin JT, Phosphorylation of the N-ethylmaleimide-sensitive factor isassociated with depolarization-dependent neurotransmitter release from synaptosomes. J. Biol. Chem. 2001; 276:12174–12181.

McMahon HT, Bolshakov VY, Janz R, Hammer RE, Siegelbaum SA, Südhof TC. Synaptophysin, a major synaptic vesicle protein, is not essential for neurotransmitter release. Proc Natl Acad Sci USA. 1996;93(10):4760–4.

Melland H, Carr EM, Gordon SL. Disorders of synaptic vesicle fusion machinery. J Neurochem. 2021;157(2):130–64.

Misura KM, Scheller RH, Weis WI. Three-dimensional structure of the neuronal-Sec1-syntaxin 1a complex. Nature. 2000;404(6776):355–62.

Mosalaganti S, Obarska-Kosinska A, Siggel M, Taniguchi R, Turoňová B, Zimmerli CE, et al. AI-based structure prediction empowers integrative structural analysis of human nuclear pores. Science. 2022;376(6598):eabm9506.

Murthy VN, Stevens CF. Reversal of synaptic vesicle docking at central synapses. Nat Neurosci. 1999;2(6):503–7.

Nair D, Hosy E, Petersen JD, Constals A, Giannone G, Choquet D, et al. Super-resolution imaging reveals that AMPA receptors inside synapses are dynamically organized in nanodomains regulated by PSD95. J Neurosci. 2013;33(32):13204–24.

Neher E, Brose N. Dynamically primed synaptic vesicle states: key to understand synaptic short-term plasticity. Neuron. 2018;100(6):1283–91.

Orozco-Borunda DH, Papantoniou C, Brose N, Lucic V. Direct cryo-ET detection of native SNARE and Munc13 protein bridges using AI classification and preprocessing. bioRxiv. 2025. https://doi.org/10.1101/2024.12.18.629213.

Papantoniou C, Laugks U, Betzin J, Capitanio C, Ferrero JJ, Sánchez-Prieto J, et al. Munc13- and SNAP25-dependent molecular bridges play a key role in synaptic vesicle priming. Sci Adv. 2023;9(25):eadf6222.

Parisotto D, Pfau M, Scheutzow A, Wild K, Mayer MP, Malsam J, et al. An extended helical conformation in domain 3a of Munc18-1 provides a template for SNARE (soluble N-ethylmaleimide-sensitive factor attachment protein receptor) complex assembly. J Biol Chem. 2014;289(14):9639–50.

Park D, Fujise K, Wu Y, Luján R, Del Olmo-Cabrera S, Wesseling JF, et al. Overlapping role of synaptophysin and synaptogyrin family proteins in determining the small size of synaptic vesicles. Proc Natl Acad Sci USA. 2024;121(29):e2409605121.

Pérez-Lara Á, Thapa A, Nyenhuis SBB, Nyenhuis DAA, Halder P, Tietzel M, et al. PtdInsP $_2$ and PtdSer cooperate to trap synaptotagmin-1 to the plasma membrane in the presence of calcium. elife. 2016;5:1–22.

Peters JJ, Leitz J, Guo Q, Beck F, Baumeister W, Brunger AT. A feature-guided, focused 3D signal permutation method for subtomogram averaging. J Struct Biol. 2022;214(2):107851.

Prinslow EA, Stepien KP, Pan YZ, Xu J, Rizo J. Multiple factors maintain assembled trans-SNARE complexes in the presence of NSF and αSNAP. elife [Internet]. 2019;8:e38880. Available from: https://elifesciences.org/articles/38880.

Quade B, Camacho M, Zhao X, Orlando M, Trimbuch T, Xu J, et al. Membrane bridging by Munc13-1 is crucial for neurotransmitter release. elife [Internet]. 2019;8:e42806. Available from: https://elifesciences.org/articles/42806.

Radhakrishnan A, Li X, Grushin K, Krishnakumar SS, Liu J, Rothman JE. Symmetrical arrangement of proteins under release-ready vesicles in presynaptic terminals. Proc Natl Acad Sci USA. 2021;118(5):e2024029118.

Raghavachari S, Lisman JE. Properties of quantal transmission at CA1 synapses. J Neurophysiol. 2004;92(4):2456–67.

Raja MK, Preobraschenski J, Del Olmo-Cabrera S, Martinez-Turrillas R, Jahn R, Perez-Otano I, et al. Elevated synaptic vesicle release probability in synaptophysin/gyrin family quadruple knockouts. elife. 2019;8:1–23.

Rizo J. Molecular mechanisms underlying neurotransmitter release. Annu Rev Biophys. 2022;51(1):377–408.

Rothman JE. The principle of membrane fusion in the cell (Nobel lecture). Angew Chem Int Ed. 2014;53(47):12676–94.

Ryu JK, Min D, Rah SH, Kim SJ, Park Y, Kim H, et al. Spring-loaded unraveling of a single SNARE complex by NSF in one round of ATP turnover. Science. 2015;347(6229):1485–9.

Sakamoto H, Ariyoshi T, Kimpara N, Sugao K, Taiko I, Takikawa K, et al. Synaptic weight set by Munc13-1 supramolecular assemblies. Nat Neurosci. 2018;21(1):41–9.

Schuller AP, Wojtynek M, Mankus D, Tatli M, Kronenberg-Tenga R, Regmi SG, et al. The cellular environment shapes the nuclear pore complex architecture. Nature. 2021;598(7882):667–71.

Shu T, Jin H, Rothman JE, Zhang Y. Munc13-1 MUN domain and Munc18-1 cooperatively chaperone SNARE assembly through a tetrameric complex. Proc Natl Acad Sci USA. 2020;117(2):1036–41.

Sieber JJ, Willig KI, Kutzner C, Gerding-Reimers C, Harke B, Donnert G, et al. Anatomy and dynamics of a supramolecular membrane protein cluster. Science. 2007;317(5841):1072–6.

Silva M, Tran V, Marty A. Calcium-dependent docking of synaptic vesicles. Trends Neurosci. 2021;44(7):579–92.

Sinha R, Ahmed S, Jahn R, Klingauf J. Two synaptobrevin molecules are sufficient for vesicle fusion in central nervous system synapses. Proc Natl Acad Sci USA. 2011;108(34):14318–23.

Stepien KP, Prinslow EA, Rizo J. Munc18-1 is crucial to overcome the inhibition of synaptic vesicle fusion by αSNAP. Nat Commun. 2019;10(1):4326.

Stepien KP, Xu J, Zhang X, Bai XC, Rizo J. SNARE assembly enlightened by cryo-EM structures of a synaptobrevin–Munc18-1–syntaxin-1 complex. Sci Adv. 2022;8:eabo5272.

Südhof TC. The presynaptic active zone. Neuron. 2012;75(1):11–25.

Südhof TC. Neurotransmitter release: the last millisecond in the life of a synaptic vesicle. Neuron. 2013;80(3):675–90.

Südhof TC. Synaptic neurexin complexes: a molecular code for the logic of neural circuits. Cell. 2017;171(4):745–69.

Sutton RBB, Fasshauer D, Jahn R, Brunger AT. Crystal structure of a SNARE complex involved in synaptic exocytosis at 2.4 Å resolution. Nature. 1998;395(6700):347–53.

Takamori S, Holt M, Stenius K, Lemke EA, Grønborg M, Riedel D, et al. Molecular anatomy of a trafficking organelle. Cell. 2006;127(4):831–46.

Tang AH, Chen H, Li TP, Metzbower SR, MacGillavry HD, Blanpied TA. A trans-synaptic nanocolumn aligns neurotransmitter release to receptors. Nature [Internet]. 2016;536:210–4. Available from: http://www.nature.com/doifinder/10.1038/nature19058.

Tegunov D, Cramer P. Real-time cryo-electron microscopy data preprocessing with Warp. Nat Methods. 2019;16(11):1146–52.

Tegunov D, Xue L, Dienemann C, Cramer P, Mahamid J. Multi-particle cryo-EM refinement with M visualizes ribosome-antibiotic complex at 3.5 Å in cells. Nat Methods. 2021;18(2):186–93.
Toulmé E, Salazar Lázaro A, Trimbuch T, Rizo J, Rosenmund C. Neurotransmitter release is triggered by a calcium-induced rearrangement in the synaptotagmin-1/SNARE complex primary interface. Proc Natl Acad Sci USA. 2024;121(42):e2409636121.
Trimbuch T, Xu J, Flaherty D, Tomchick DR, Rizo J, Rosenmund C. Re-examining how complexin inhibits neurotransmitter release. elife. 2014;3:e02391.
Turk M, Baumeister W. The promise and the challenges of cryo-electron tomography. FEBS Lett. 2020;594(20):3243–61.
Voleti R, Jaczynska K, Rizo J. Ca2+-dependent release of synaptotagmin-1 from the SNARE complex on phosphatidylinositol 4,5-bisphosphate-containing membranes. elife [Internet]. 2020;9:e57154. Available from: https://elifesciences.org/articles/57154.
Wang S, Li Y, Gong J, Ye S, Yang X, Zhang R, et al. Munc18 and Munc13 serve as a functional template to orchestrate neuronal SNARE complex assembly. Nat Commun. 2019;10(1):69.
Wang Z, Grange M, Pospich S, Wagner T, Kho AL, Gautel M, et al. Structures from intact myofibrils reveal mechanism of thin filament regulation through nebulin. Science. 2022a;375(6582):eabn1934.
Wang CS, Chanaday NL, Monteggia LM, Kavalali ET. Probing the segregation of evoked and spontaneous neurotransmission via photobleaching and recovery of a fluorescent glutamate sensor. elife. 2022b;11:e76008.
Wang C, Jiang W, Leitz J, Yang K, Esquivies L, Wang X, et al. Structure and topography of the synaptic V-ATPase–synaptophysin complex. Nature [Internet]. 2024;631(8022):899–904. Available from: https://www.nature.com/articles/s41586-024-07610-x.
Watanabe S, Trimbuch T, Camacho-Pérez M, Rost BR, Brokowski B, Söhl-Kielczynski B, et al. Clathrin regenerates synaptic vesicles from endosomes. Nature [Internet]. 2014;515:228–33. Available from: http://www.nature.com/doifinder/10.1038/nature13846.
Weber T, Zemelman BV, McNew JA, Westermann B, Gmachl M, Parlati F, et al. SNAREpins: minimal machinery for membrane fusion. Cell. 1998;92(6):759–72.
Weninger K, Bowen ME, Chu S, Brunger AT. Single-molecule studies of SNARE complex assembly reveal parallel and antiparallel configurations. Proc Natl Acad Sci USA. 2003;100(25):14800–5.
White KI, Zhao M, Choi UB, Pfuetzner RA, Brunger AT. Structural principles of SNARE complex recognition by the AAA+ protein NSF. elife [Internet]. 2018;7:e38888. Available from: https://elifesciences.org/articles/38888.
White KI, Khan YA, Qiu K, Balaji A, Choi UB, Couoh S, et al. Structural remodeling of target-SNARE protein complexes by NSF enables synaptic transmission. Nat Commun. 2025; 16:8371.
Wittig S, Ganzella M, Barth M, Kostmann S, Riedel D, Pérez-Lara Á, et al. Cross-linking mass spectrometry uncovers protein interactions and functional assemblies in synaptic vesicle membranes. Nat Commun. 2021;12(1):858.
Xu J, Camacho M, Xu Y, Esser V, Liu X, Trimbuch T, et al. Mechanistic insights into neurotransmitter release and presynaptic plasticity from the crystal structure of Munc13-1 C 1 C 2 BMUN. elife [Internet]. 2017;6:e22567. Available from: http://elifesciences.org/lookup/doi/10.7554/eLife.22567.
Yang X, Wang S, ShengY, Zhang M, Zou W, Wu L, et al. Syntaxin opening by the MUN domain underlies the function of Munc13 in synaptic-vesicle priming. Nat Struct Mol Biol. 2015;22(7):547–54.
Yousuf A. Khan, K. Ian White & Axel T. Brunger. The AAA+ superfamily:a review of the structural and mechanistic principles of these molecular machines, Critical Reviews in Biochemistry andMolecular Biology, 2021;57(2):156–187. https://doi.org/10.1080/10409238.2021.1979460.

Zhou, H. et al. Toward a comprehensive characterization of a human cancer cell phosphoproteome. J. Proteome Res. 2013;12, 260–271.
Zhao M, Wu S, Zhou Q, Vivona S, Cipriano DJ, Cheng Y, et al. Mechanistic insights into the recycling machine of the SNARE complex. Nature. 2015;518(7537):61–7.
Zhou Q, Lai Y, Bacaj T, Zhao M, Lyubimov AY, Uervirojnangkoorn M, et al. Architecture of the synaptotagmin–SNARE machinery for neuronal exocytosis. Nature. 2015;525(7567):62–7.
Zhou Q, Zhou P, Wang AL, Wu D, Zhao M, Südhof TC, et al. The primed SNARE–complexin–synaptotagmin complex for neuronal exocytosis. Nature. 2017;548(7668):420–5.

Open Access This chapter is licensed under the terms of the Creative Commons Attribution 4.0 International License (http://creativecommons.org/licenses/by/4.0/), which permits use, sharing, adaptation, distribution and reproduction in any medium or format, as long as you give appropriate credit to the original author(s) and the source, provide a link to the Creative Commons license and indicate if changes were made.

The images or other third party material in this chapter are included in the chapter's Creative Commons license, unless indicated otherwise in a credit line to the material. If material is not included in the chapter's Creative Commons license and your intended use is not permitted by statutory regulation or exceeds the permitted use, you will need to obtain permission directly from the copyright holder.

